

Free energy landscape of mechanically unfolded model proteins: extended Jarzynski versus inherent structure reconstruction

Stefano Luccioli,^{1,2,*} Alberto Imparato,^{3,†} and Alessandro Torcini^{1,2,4,‡}

¹*Istituto dei Sistemi Complessi, CNR, via Madonna del Piano 10, I-50019 Sesto Fiorentino, Italy*

²*INFN, Sez. Firenze, and CSDC, via Sansone, 1 - I-50019 Sesto Fiorentino, Italy*

³*Dipartimento di Fisica, INFN-Sezione di Torino,*

CNISM-Sezione di Torino, Politecnico di Torino,

Corso Duca degli Abruzzi 24, 10129 Torino, Italy

⁴*Centre de Physique Théorique, Campus de Luminy, 13288 Marseille, France*

The equilibrium free energy landscape of off-lattice model heteropolymers as a function of an internal coordinate, namely the end-to-end distance, is reconstructed from out-of-equilibrium steered molecular dynamics data. This task is accomplished via two independent methods: by employing an extended version of the Jarzynski equality (EJE) and the inherent structure (IS) formalism. For a sequence with good foldability properties, a quantitative agreement between the free energies obtained with the two schemes is observed in a range of temperatures around the “folding transition”. Moreover, for this sequence the mechanically induced structural transitions can be related to thermodynamical aspects of folding. However, for a random sequence the IS reconstruction is unable to well reproduce the free energy landscape, since in this case the main contribution to entropic terms cannot be ascribed to vibrational fluctuations around the ISs, but to large conformational rearrangements.

PACS numbers: 87.15.Aa,82.37.Rs,05.90.+m

I. INTRODUCTION

Several states of matter are characterized by a non trivial free energy landscape (FEL), which can be at the origin of peculiar structural and dynamical features. Supercooled liquids, glasses, atomic clusters and biomolecules [1] are typical examples of systems whose thermodynamical behavior can be traced back to the intricate topological properties of the underlying FEL. The pioneering work by Stillinger and Weber on inherent structures (ISs) of liquids [2] revealed the importance of investigating the stationary points of the potential energy surface (PES) for characterizing their dynamical and thermodynamical properties. Similar approaches have been proposed and successfully applied, in glasses [3] and supercooled liquids [4], to the identification of the structural-arrest temperature. This temperature marks a topological transition from a dynamics evolving in a landscape dominated by minima to one where unstable saddles play a major role [4, 5].

More recently, this kind of analysis has been applied to the study of protein models [1, 6, 7, 8, 9, 10, 11]. In particular, several studies have been devoted to the reconstruction of the PES and of the FEL topology in terms of graphs (at various levels of coarse graining) connecting the folded states to the unfolded structures [6, 7, 8]. The knowledge of the graph structure connecting the various metastable states and of the probability transitions among them allows for a reconstruction of the folding dynamics in terms of a master equation [12]. Moreover, detailed analysis of the thermodynamical and dynamical features, characteristics of proteins, have been quite recently carried out in terms of ISs [9, 10, 11]. These analysis suggest that the folding process of a protein towards its native configuration depends crucially on the structure and topological properties of its (free) energy landscape. Confirming somehow the conjecture that the FEL of a protein has a funnel-like shape: the native configuration being located inside the so-called native valley at the bottom of the funnel itself [13].

On the other hand, mechanical unfolding of single biomolecules represents a powerful technique to extract information on their internal structure as well as on their unfolding and refolding pathways [14, 15, 16, 17, 18]. However, mechanical unfolding of biomolecules is an out-of-equilibrium process: unfolding events occur on time scales much shorter than the typical relaxation time of the molecule towards equilibrium. Nonetheless, by using the equality introduced by Jarzynski [19], the free energy of mechanically manipulated biomolecules can be recovered as a function of

*Electronic address: stefano.luccioli@fi.isc.cnr.it

†Electronic address: alberto.imparato@polito.it

‡Electronic address: alessandro.torcini@cnr.it

an externally controlled parameter [20, 21]. Moreover, an extended version of the Jarzynski equality (EJE) has been proposed in order to estimate the equilibrium free energy landscape in absence of applied forces as a function of an internal coordinate of the system (usually, the end-to-end distance ζ) [22, 23, 24, 25]. Quite recently this approach has been successfully applied to data obtained from nanomanipulation of titin I27 domain with Atomic Force Microscopy (AFM) [26] and from steered molecular dynamics simulations of a mesoscopic off-lattice protein model [27]. The analysis reported in [27] was devoted to a single sequence previously identified as a reasonably fast folder [28, 29] and it was essentially performed at a unique temperature.

As an extension of the analysis performed in Ref. [27], in the present paper we reconstruct, for two different sequences with bad and good folding properties, the equilibrium FEL as a function of the end-to-end distance ζ in two distinct ways: namely, by employing the EJE approach and the IS distributions. We will show that specific features of the landscapes characteristic of a protein, i.e. a good folder, can be singled out from a comparison of the two approaches. Furthermore, the different unfolding structural transitions can be associated to the detachment of specific strands of the examined heteropolymers. In particular, the investigation of the IS distributions allows us to give an estimate of the energetic and entropic barriers separating the native state from the completely stretched configuration. Moreover, for the good folder the temperature dependence of the free energy barrier heights and the unfolding times can be related.

An important aspect to clarify is the relationship between the thermal and mechanical unfolding pathways of proteins: experimental [30] as well as numerical works [31, 32] seem to suggest that these paths are indeed different. However, there are indications that the thermal paths can be recovered also via the manipulation procedure in the limit of very low pulling velocities [32]. This seems to be in agreement with our findings for the good folder, which indicate that the observed structural transitions, induced by mechanical unfolding, can be put in direct relationship with the thermal transitions usually identified for the folding/unfolding process.

The paper is organized as follows, Sect. II is devoted to the introduction of the employed model and sequences, as well as of the simulation protocols. The inherent structure formalism and the extended Jarzynski equality are briefly illustrated in Sect. III and Sect. IV, respectively. The thermodynamical properties of the studied sequences are reported in Sect. V. While Sect. VI (resp. Sect. VII) is devoted to the free energy landscape reconstruction in terms of the extended Jarzynski equality (resp. inherent structure approach). In Sect. VII the two methods are also compared and discussed. Finally, the results are summarized in Sect. VIII, while in an Appendix we report a concise comparison of the tail-pulled protocol versus the head-pulled one.

II. MODEL AND SIMULATION PROTOCOL

A. The model

The model studied in this paper is a modified version of the 3d off-lattice model introduced by Honeycutt-Thirumalai [33] and successively generalized by Berry *et al.* to include a harmonic interaction between next-neighbouring beads instead of rigid bonds [34]. This model has been widely studied in the context of thermally driven folding and unfolding [8, 10, 28, 29, 33, 34, 35, 36] and only more recently for what concerns mechanical folding and refolding [37, 38]. The model consists of a chain of L point-like monomers mimicking the residues of a polypeptidic chain. For the sake of simplicity, only three types of residues are considered: hydrophobic (B), polar (P) and neutral (N) ones.

The intramolecular potential is composed of four terms: a stiff nearest-neighbour harmonic potential, V_1 , intended to maintain the bond distance almost constant, a three-body interaction V_2 , which accounts for the energy associated to bond angles, a four-body interaction V_3 corresponding to the dihedral angle potential, and a long-range Lennard-Jones (LJ) interaction, V_4 , acting on all pairs i, j such that $|i - j| > 2$, namely

$$V_1(r_{i,i+1}) = \alpha(r_{i,i+1} - r_0)^2, \quad (1)$$

$$V_2(\theta_i) = A \cos(\theta_i) + B \cos(2\theta_i) - V_0, \quad (2)$$

$$V_3(\varphi_i, \theta_i, \theta_{i+1}) = C_i[1 - S(\theta_i)S(\theta_{i+1})\cos(\varphi_i)] + D_i[1 - S(\theta_i)S(\theta_{i+1})\cos(3\varphi_i)], \quad (3)$$

$$V_4(r_{i,j}) = \varepsilon_{i,j} \left(\frac{1}{r_{i,j}^{12}} - \frac{c_{i,j}}{r_{i,j}^6} \right) \quad (4)$$

Here, $r_{i,j}$ is the distance between the i -th and the j -th monomer, θ_i and φ_i are the bond and dihedral angles at the i -th monomer, respectively. The parameters $\alpha = 50$ and $r_0 = 1$ (both expressed in adimensional units) fix the strength of the harmonic force and the equilibrium distance between subsequent monomers (which, in real proteins, is of the order of a few Å). The value of α is chosen to ensure a value for V_1 much larger than the other terms of potential in order to reproduce the stiffness of the protein backbone. The expression for the bond-angle potential

term $V_2(\theta_i)$ (2) corresponds, up to the second order, to a harmonic interaction term $\sim (\theta_i - \theta_0)^2/2$, where

$$A = -k_\theta \frac{\cos(\theta_0)}{\sin^2(\theta_0)}, \quad B = \frac{k_\theta}{4 \sin^2(\theta_0)}, \quad V_0 = A \cos(\theta_0) + B \cos(2\theta_0) \quad , \quad (5)$$

with $k_\theta = 20\epsilon_h$, $\theta_0 = 5\pi/12$ rad or 75° and where ϵ_h sets the energy scale. This formulation in terms of cosines allows to speed up the simulation, since it is sufficient to evaluate $\cos(\theta_i)$ and the value of bond-angle is not needed, and at the same time to avoid spurious divergences in the force expression due to the vanishing of $\sin(\theta_i)$ when three consecutive atoms become aligned [39].

The dihedral angle potential is characterized by three minima for $\varphi = 0$ (associated to a so-called *trans state*) and $\varphi = \pm 2\pi/3$ (corresponding to *gauche states*), this potential is mainly responsible for the formation of secondary structures. In particular large values of the parameters C_i, D_i favor the formation of *trans state* and therefore of β -sheets, while when *gauche states* prevail α -helices are formed. The parameters (C_i, D_i) have been chosen as in [35], i.e. if two or more beads among the four defining φ are neutral (N) then $C_i = 0$ and $D_i = 0.2\epsilon_h$, in all the other cases $C_i = D_i = 1.2\epsilon_h$. The *tapering function* $S(\theta_i) = 1 - \cos^3(\theta_i)$ has been introduced in the expression of V_3 in order to cure a well known problem in the dihedral potentials [39]. This problem is encountered whenever $\theta_i = 0$ or π , i.e. when three consecutive beads are in the same line, in these situations the associated dihedral angle is no more defined and a discontinuity in V_3 arises. In contrast to what reported in [39] this situation is not improvable for the present model. The quantity $S(\theta_i)S(\theta_{i+1})$ entering in the definition of V_3 has a limited influence on the dynamics apart in proximity of the above mentioned extreme cases. Moreover, $S(\theta_i)S(\theta_{i+1})$ is C^∞ , its value is essentially one almost for any θ_i , it does not introduce any extra minima in the potential and it vanishes smoothly for $\theta_i \rightarrow 0$ or $\theta_i \rightarrow \pi$ [40].

The last term V_4 has been introduced to mimic effectively the interactions with the solvent, it is a Lennard-Jones potential and it depends on the type of interacting residues as follows:

- if any of the two monomers is neutral the potential is repulsive $c_{N,X} = 0$ and its scale of energy is fixed by $\epsilon_{N,X} = 4\epsilon_h$;
- for interactions between hydrophobic residues $c_{B,B} = 1$ and $\epsilon_{B,B} = 4\epsilon_h$;
- for any polar-polar or polar-hydrophobic interaction $c_{P,P} \equiv c_{P,B} = -1$ and $\epsilon_{P,P} \equiv \epsilon_{P,B} = (8/3)\epsilon_h$.

Accordingly, the Hamiltonian of the system reads

$$H = K + V = \sum_{i=1}^L \frac{p_{x,i}^2 + p_{y,i}^2 + p_{z,i}^2}{2} + \sum_{i=1}^{L-1} V_1(r_{i,i+1}) + \sum_{i=2}^{L-1} V_2(\theta_i) + \sum_{i=2}^{L-2} V_3(\varphi_i, \theta_i, \theta_{i+1}) + \sum_{i=1}^{L-3} \sum_{j=i+3}^L V_4(r_{ij}) \quad (6)$$

where, for the sake of simplicity, all monomers are assumed to have the same unitary mass, the momenta are defined as $(p_{x,i}, p_{y,i}, p_{z,i}) \equiv (\dot{x}_i, \dot{y}_i, \dot{z}_i)$ and we fix $\epsilon_h = 1$.

In the present paper we consider the two following sequences of 46 monomers,

- [GF]= $B_9N_3(PB)_4N_3B_9N_3(PB)_5P$ a sequence that has been widely analyzed in the past for spontaneous folding [8, 10, 28, 29, 33, 34, 35, 36] as well as for mechanical unfolding and refolding [37, 38];
- [BF]= $BNBPPB_3NPB_4NBPB_2NP_2B_5N_2BPBPNP_2NBP_2BNB_2PB_2$ a randomly generated sequence, but with the same number of B, P and N monomers as the *GF*.

These two sequences have been chosen because *GF* has been previously identified as a reasonably fast folder [28] (see also [34] for a detailed and critical analysis of the basin-bottom structures observed for this model), while we expect that the sequence *BF*, being randomly chosen, cannot have the characteristic of a good folder. From now on we refer to the sequence *GF* (resp. *BF*) as the *good* (resp. *bad*) folder.

The 46-mer sequence *GF* exhibits a four stranded β -barrel Native Configuration (NC) with an associated potential energy $E_{NC} = -49.878$. Please note that the model is here analyzed by employing the same potential and parameter set reported in Ref. [35], but neglecting any diversity among the hydrophobic residues. The NC is stabilized by the attractive hydrophobic interactions among the *B* residues, in particular the first and third B_9 strands, forming the core of the NC, are parallel to each other and anti-parallel to the second and fourth strand, namely, $(PB)_4$ and $(PB)_5P$. The latter strands are exposed towards the exterior due to the presence of polar residues.

The native structure of the *BF* is quite different, it has a core constituted by the first three β -strands and a very long "tail" (made of 18 residues) wrapped around the core. In particular, the first and second β -strand (namely,

	GF	BF
V_{NC}	-49.878	-23.956
V_1	0.787	0.777
V_2	1.767	5.744
V_3	2.602	23.105
V_4	-55.035	-53.582

TABLE I: Potential energy values associated to the NC of the GF and BF, the different contributions to the total potential energy V_{NC} are also reported.

$BNBPB_3NP$ and B_4NBPB_2) are formed by 9 residues, and anti-parallel to each other, almost lying in a plane. The third strand (namely, P_2B_5) is made of 7 residues and it is located in a plane lying in-between the first and second strand and almost perpendicular to the plane of the first 2 strands. The chain rotates of almost 90 degrees in correspondence of the two consecutive neutral beads and then exhibits a short strand of 3 beads PBP before turning back with a parallel strand of 7 beads (PB_2NBP_2) that passes below the plane formed by the first 2 strands. Finally the chain turns once more back by passing this time above the plane of the 2 first strands. In the final part of the tail of the chain a short strand of 5 residues, parallel to the 4-th and 5-ones, can be identified as B_2PB_2 . The potential energy of the NC of the BF is quite high with respect to the GF , namely $V_{NC} = -23.956$. Moreover, this difference, as reported in Table I, is essentially due to the difference in the dihedral contributions, that is much higher in the NC of the BF with respect to the GF , while all the other contributions, in particular the LJ ones, have nearby values. The dihedral contribution that arises in the BF is essentially due to the arrangement of the first 3 strands, since the structure of the NC in this part of the chain lies over two almost orthogonal planes.

B. Simulation protocol: equilibrium Langevin dynamics

Molecular dynamics (MD) canonical simulations at equilibrium temperature T have been performed by integrating the corresponding Langevin equation for each monomer of unitary mass (characterized by the position vector \mathbf{r}_i):

$$\ddot{\mathbf{r}}_i = \mathbf{F}(\mathbf{r}_i) - \gamma \dot{\mathbf{r}}_i + \eta(t) \quad i = 1, L \quad (7)$$

where $\eta(t)$ is a zero average Gaussian noise term with correlations given by $\langle \eta_\alpha(t) \eta_\beta(t') \rangle = 2T\gamma\delta(t-t')\delta_{\alpha,\beta}$; $\mathbf{F} = -\nabla V$, being V the intramolecular potential introduced in II A, γ the friction coefficient associated to the solvent and by assuming an unitary Boltzmann constant.

Numerical integrations have been implemented via a standard Euler scheme with a time-step $\Delta t = 0.005$ and with a low friction coefficient $\gamma = 0.05$ [35]. Two different kinds of MD have been performed, namely unfolding simulations (US) and folding simulations (FS). In the first case the initial state of the system is taken equal to the native configuration (NC), that we assume to coincide with the minimal energy configuration. In the latter one the initial state is a completely unfolded configuration.

C. Simulation protocol: out-of-equilibrium mechanical unfolding

In order to mimic the mechanical pulling of the protein attached to a AFM cantilever, or analogously when trapped in an optical tweezer, one extremum of the chain was kept fixed and the last bead is attached to a pulling apparatus with a spring of elastic constant k . The external force is applied by moving the "cantilever" along a fixed direction with a certain protocol $z(t)$. Before pulling the protein, the coordinate system is always rigidly rotated, in order to have the z-axis aligned along the end-to-end direction connecting the first and last bead. Therefore by denoting with ζ the end-to-end distance the component of the external force along this direction reads as

$$F_{ext} = k(z - \zeta) \quad (8)$$

where $k = 10$ in order to suppress fast oscillations. As recently pointed out it is extremely important to use a sample of thermally equilibrated initial configurations to correctly reproduce the equilibrium FEL via the JE. [21]. Therefore, before pulling the protein, we have performed a thermalization procedure in two steps. At a fixed temperature T , initially the protein evolves freely starting from the NC for a time $t = 1,000$, then it is attached to the external

apparatus, with the first bead blocked, and it equilibrates for a further for a further time period $t = 500$. The system (at sufficiently low temperatures) quickly settles down to a "native-like" configuration. This configuration is then employed as the starting state for the forced folding. The protocol that we have used is a linear pulling protocol with a constant speed v_p , i.e. $z(t) = z(0) + v_p \times t$, by assuming that the pulling starts at $t = 0$. Usually we have employed velocities $v_p \in [5 \times 10^{-5} : 5 \times 10^{-2}]$ and set $z(0) = \zeta_0$, i.e. to the end-to-end distance associated to the native configuration.

III. INHERENT STRUCTURE FORMALISM

Inherent structures correspond to local minima of the potential energy, in particular the phase space visited by the protein during its dynamical evolution can be decomposed into disjoint attraction basin, each corresponding to a specific IS. Therefore, the canonical partition function can be expressed within the IS formalism as a sum over the non overlapping basins of attraction, each corresponding to a specific minimum (IS) a [1, 9]:

$$Z_{IS}(T) = \frac{1}{\lambda^{3N'}} \sum_a e^{-\beta V_a} \int_{\Gamma_a} e^{-\beta \Delta V_a(\Gamma)} d\Gamma = \sum_a e^{-\beta[V_a + R_a(T)]} \quad (9)$$

where N' is the number of degrees of freedom of the system, λ is the thermal wavelength, $\beta = 1/T$, Γ represents one of the possible conformations of the protein within the basin of attraction of a , V_a is the potential energy associated to the minimum a , $\Delta V_a(\Gamma) = V(\Gamma) - V_a$ and $R_a(T)$ the vibrational free energy due to the fluctuations around the minimum.

The vibrational term $R_a(T)$ can be estimated by assuming a harmonic basin of attraction:

$$e^{-\beta R_a(T)} = \frac{1}{\lambda^{3N-6}} \int_{\Gamma_a} e^{-\beta \Delta V_a(\Gamma)} d\Gamma = \prod_{j=1}^{3N-6} \frac{T}{\omega_a^j} \quad (10)$$

where ω_a^j are the frequencies of the vibrational modes around the IS a and an unitary reduced Planck constant has been considered.

Therefore the probability to be in the basin of attraction of the IS a is

$$p_a(T) = \frac{1}{Z_{IS}(T)} e^{-\beta(V_a + R_a(T))} \quad (11)$$

The free energy of the whole system at equilibrium is simply given by $f_{IS}(T) = -T \ln[Z_{IS}(T)]$. However if one is interested to construct a free energy landscape as a function of a parameter characterizing the different IS, like e.g. the Kabsch distance δ_K [41] or the end-to-end distance ζ , this is possible by defining a partition function restricted to IS with an end-to-end distance within the narrow interval $[\zeta; \zeta + d\zeta]$

$$Z_{IS}(\zeta, T) = \sum_a' e^{-\beta[V_a + R_a(T)]} \quad (12)$$

where the \sum' indicates that the sum is not over the whole ensemble of ISs $\{a\}$ but restricted. The free energy profile as a function of ζ can be simply obtained by the relationship:

$$f_{IS}(\zeta, T) = -T \ln[Z_{IS}(\zeta, T)] \quad ; \quad (13)$$

while the average potential and free vibrational energy, corresponding to ISs characterized by a certain ζ , can be estimated as follows:

$$V_{IS}(\zeta, T) = \frac{\sum_a' V_a e^{-\beta[V_a + R_a(T)]}}{Z_{IS}(\zeta, T)} \quad ; \quad R_{IS}(\zeta, T) = \frac{\sum_a' R_a(T) e^{-\beta[V_a + R_a(T)]}}{Z_{IS}(\zeta, T)} \quad (14)$$

In order to find the different ISs one can perform MC samplings or molecular dynamics (MD) simulations. We have chosen to examine MD trajectories at constant temperature via a Langevin integration scheme. In particular, we have built up two data banks of ISs: the thermal data bank (TDB) obtained by performing equilibrium canonical simulations and the pulling data bank (PDB) by mechanically unfolding the protein. In order to find the different ISs the equilibrium (resp. out-of-equilibrium) Langevin trajectory is sampled at constant time intervals $\delta t = 5$ (resp. at constant elongation increments $\delta \zeta = 0.1$) to pinpoint a series of configurations, which afterward are relaxed via

T	goodfolder	badfolder
0.1	2,843	456
0.2	5,875	1,763
0.3	12,359	6,477
0.4	35,409	21,060
0.5	52,546	45,950
0.6	51,971	—
0.7	54,736	—

TABLE II: Number of distinct ISs contained in the PBD at different temperatures. These have been obtained by sampling, during out-of-equilibrium mechanical unfoldings, several Langevin trajectories at constant elongation increments $\delta\zeta = 0.1$. The total number of relaxations performed for each temperature amounts to $\sim 60,000$ corresponding to ~ 200 repetitions of the same pulling experiment. For the bad folder not all temperatures have been examined.

a steepest descent dynamics and finally refined by means of a standard Newton's method. In the case of the TDB, in order to speed up the search of ISs we have employed a so-called "quasi-Newton" method [42]¹. For mechanical unfolding, the protein is unblocked and the pulling apparatus removed before the relaxation stage. Two local minima are identified as distinct whenever their energies differ more than 1×10^{-5} . The TDB for the good (resp. bad) folder contains 579,749 (resp. 210,782) distinct ISs collected via equilibrium simulations at various temperatures in the range $[0.3; 2.0]$. The PDB contains 3,000 – 50,000 ISs depending on the examined temperature as detailed in the Table II.

IV. EXTENDED JARZYNSKI EQUALITY

In the present section, we discuss an extended version of the Jarzynski equality, which allows to obtain the free energy profile as a function of a collective coordinate. Let x be the variable that identifies the system microscopic state, e.g. the collection of the positions and momenta of all the particles in the system $x = \{\mathbf{r}_i, \mathbf{p}_i\}$. The system Hamiltonian is a function of x , and will be indicated as $H_0(x)$ in the following.

Let $X(x)$ be a macroscopic observable of the system, e.g. the volume, whose value can be varied by applying an external force. In the following we will consider only conservative forces, and thus in order to manipulate the system, we can couple it to an external potential $U_\lambda(X)$. This is an explicit function of the observable X and it also depends on a parameter λ , whose value will be modified accordingly to a given time protocol $\lambda(t)$. Thus the system can be characterized by the time-dependent Hamiltonian $H(x, t) = H_0(x) + U_{\lambda(t)}(X(x))$. The work *done* on the system by the external potential (external force) up to time t depends on the trajectory $x(t)$ followed by the system in the phase space:

$$W_t = \int_0^t dt' \dot{\lambda}(t') \partial_\lambda U_\lambda(M(x(t')))|_{\lambda=\lambda(t')}. \quad (15)$$

Due to thermal fluctuations, W_t varies between a realization and another one of the manipulation process.

In the following we assume that the time evolution of the system is described by the following Liouville-like equation

$$\frac{\partial p(x, t)}{\partial t} = L_{\lambda(t)}(x)p(x, t), \quad (16)$$

where $L_\lambda(x)$ represents the evolution operator ruling the dynamics. The only requirement on L_λ is its compatibility with the canonical distribution associated to the Hamiltonian $H_\lambda(x) = H_0(x) + U_\lambda(M(x))$:

$$L_\lambda \frac{e^{-\beta H_\lambda(x)}}{Z_\lambda} = 0, \quad (17)$$

¹ The comparison between the steepest descent and the quasi-Newton methods has revealed that this second minimization scheme is somehow faster (1.8 times faster at $T = 0.5$ for the good folder), but while the steepest descent algorithm is able to identify the metastable stationary states in the 99.8 % of examined cases the quasi-Newton scheme was successful in the 98.7 % of situations. However the distributions of the identified minima (by considering the same trajectory) obtained with the two schemes were essentially coincident.

where $Z_\lambda = \int dx e^{-\beta H_\lambda(x)}$. Let us introduce the joint probability distribution $\phi(x, W, t)$ that the system is found in state x , having subjected to a work W , at time t . The time evolution of this function is governed by the partial differential equation [22, 23, 24, 25]

$$\frac{\partial \phi}{\partial t} = L_{\lambda(t)} \phi - \dot{\lambda}(t) [\partial_\lambda U_{\lambda(t)}(M(x))] \frac{\partial \phi}{\partial W}. \quad (18)$$

Assuming that the system is initially at equilibrium for vanishing external force, the initial condition of eq. (18) reads $\phi(x, W, t=0) = p_0(x)$, where $p_0(x)$ is the canonical ensemble probability distribution of the unperturbed system

$$p_0(x) = \frac{e^{-\beta H_0(x)}}{Z_0}, \quad (19)$$

and

$$Z_0 = \int dx e^{-\beta H_0(x)} \quad (20)$$

is the corresponding partition function.

We now introduce the generating function $\psi(x, \lambda, t)$ of the distribution of $\phi(x, W, t)$ defined as

$$\psi(x, \lambda, t) = \int dW e^{\lambda W} \phi(x, W, t). \quad (21)$$

The function $\psi(x, \lambda, t)$ satisfies the differential equation

$$\frac{\partial \psi}{\partial t} = L_{\lambda(t)} \psi + \dot{\lambda}(t) [\partial_\lambda U_{\lambda(t)}(M(x))] \psi. \quad (22)$$

By taking $\lambda = -\beta$, and exploiting eq. (17), it is easy to show that equation (22), with the initial condition $\psi(x, \lambda, t=0) = p_0(x)$, is identically satisfied by

$$\psi(x, -\beta, t) = \frac{e^{-\beta H(x,t)}}{Z_0}. \quad (23)$$

Integrating this relation over x one obtains the usual form of the JE:

$$\begin{aligned} \langle e^{-\beta W} \rangle_t &= \int dx \int dW e^{-\beta W} \phi(x, W, t) \\ &= \frac{Z_{\lambda(t)}}{Z_0} = \exp[-\beta (F_{\lambda(t)} - F_0)]. \end{aligned} \quad (24)$$

Here $\beta F_\lambda = -\ln Z_\lambda$ is the free energy associated to the Hamiltonian H_λ . A more general relation is obtained by multiplying both sides of eq. (23) by $\delta(X - X(x))$ before integrating over x :

$$\begin{aligned} \langle \delta(X - X(x)) e^{-\beta W} \rangle_t &= \int dx \delta(X - X(x)) \frac{e^{-\beta H(x,t)}}{Z_0} \\ &= e^{-\beta (f(X,T) + U_{\lambda(t)}(X) - F_0)}. \end{aligned} \quad (25)$$

Where $f(X, T)$ is the free energy of a constrained ensemble, in which the value $X(x)$ is fixed at X :

$$\beta f(X, T) = -\ln \int dx \delta(X - X(x)) e^{-\beta H_0(x)}. \quad (26)$$

By multiplying both sides of eq. (25) by $e^{\beta U_{\lambda(t)}(X)}$, we obtain the *extended Jarzynski equality*

$$e^{\beta U_{\lambda(t)}(X)} \langle \delta(X - X(x)) e^{-\beta W} \rangle_t = e^{-\beta (f(X,T) - F_0)}. \quad (27)$$

Equation (27) provides thus a method to evaluate the unperturbed free energy $f(X, T)$ as long as one has a reliable estimate of the lhs of this equation. The optimal estimate of $f(X, T)$ can be obtained by combining eq.(27) with the method of weighted histograms [22, 43, 44], namely

$$f(X, T) = -\frac{1}{\beta} \ln \left[\frac{\sum_t \frac{\langle \delta(X - X(x)) \exp(-\beta W_t) \rangle_t}{\langle \exp(-\beta W_t) \rangle_t}}{\sum_t \frac{\exp(-U(X,t))}{\langle \exp(-\beta W_t) \rangle_t}} \right]. \quad (28)$$

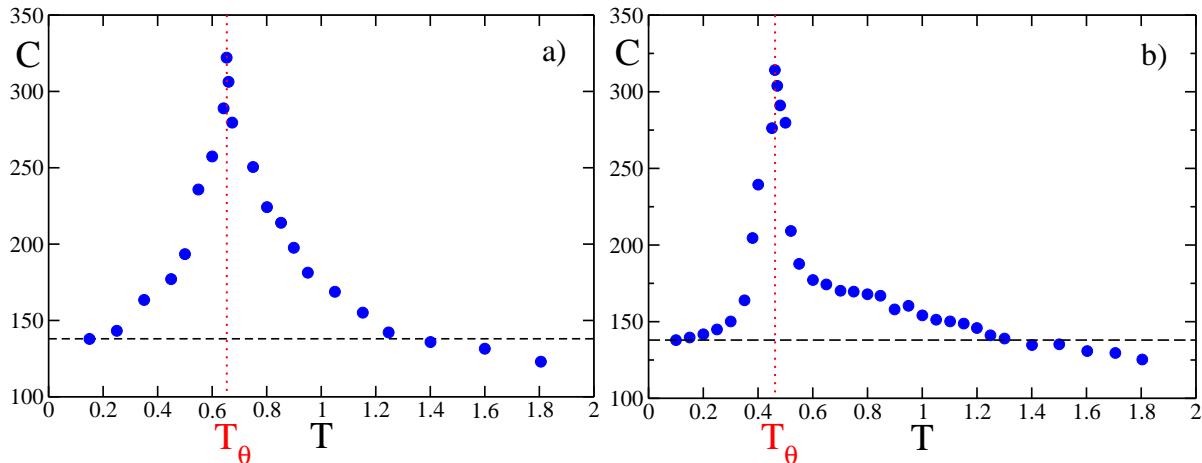


FIG. 1: (Color online) Heat capacity C as a function of the temperature T for good (a) and bad (b) folder; the vertical (red) dotted line indicates the hydrophobic collapse temperature T_θ and the horizontal (black) dashed line the value C_{sol} .

V. THERMODYNAMICAL PROPERTIES

The main thermodynamical features of the examined model can be summarized by reporting three different transition temperatures [1, 10, 11, 45, 46]: namely, the hydrophobic collapse temperature T_θ , the folding temperature T_f , and the glassy temperature T_g .

The collapse temperature discriminates between phases dominated by random-coil configurations rather than collapsed ones [47], T_θ has been usually identified as the temperature where the heat capacity $C(T)$ reaches its maximal value, namely (within the canonical formalism):

$$C(T_\theta) \equiv C^{max} \quad , \quad \text{where} \quad C(T) = \frac{\langle E^2 \rangle - \langle E \rangle^2}{T^2}, \quad (29)$$

and $\langle \cdot \rangle$ represents a time average performed over an interval $t \simeq 10^5$ by following an US trajectory. From Fig. 1, it is evident that for both sequences $C(T) \sim 138$ up to temperatures $T \sim 0.25$. This result can be understood by noticing that at low temperatures the thermal features of heteropolymers resemble that of a disordered 3D solid, with an associated heat capacity $C_{sol} \equiv 3L$. Moreover, the high temperature values are smaller than C_{sol} , since in this limit we expect that a one dimensional chain in a three dimensional space would have a specific heat $C = 2L$ [45]. However, as shown in Fig. 1, these extreme temperatures have not yet been reached. The comparison of the heat capacity curves for the GF and BF reveals that $C(T)$ obtained for the GF has a much broader peak with respect to the BF. This indicates that the transition from the NC to the random coil state is definitely sharper for the bad folder.

The folding temperature has been defined in many different ways [29, 35, 45], however we have chosen to define the folding temperature by employing the IS reconstruction of the phase space. In practice, quite long USs have been performed at various temperatures, up to duration $t = 5,000,000$. During each of this US the visited ISs have been identified at regular intervals $\delta t = 5$, and from these data we have estimated the probability $P_{nc}(T)$ to visit the NC at such temperature. The folding temperature T_f is then defined as

$$P_{nc}(T_f) \equiv 0.5 \quad . \quad (30)$$

Indeed, it should be noticed that for the GF P_{nc} is the probability to stay in the two lowest lying energy minima (ISs) and not in the NC only. These two minima can be associated to an unique attraction basin, since their energy separation is extremely small with respect to $|V_{NC}|$ (namely, 0.04) and also the corresponding configurations are almost identical, being separated by a Kabsch distance $\delta_K = 0.128$. Moreover, at any examined temperature we have always observed a rapid switching between the two configurations, indicating that there is an extremely low energy barrier among these two states.

The glassy temperature T_g indicates the temperature below which freezing of large conformational rearrangements occurs: below such a temperature the system can be trapped in local minima of the potential. By following [45], in order to locate T_g we have made a comparison among results obtained from FS and US. In particular, we have examined, at the same temperatures, the average total energy $\langle E \rangle$ of the system evaluated over finite time intervals.

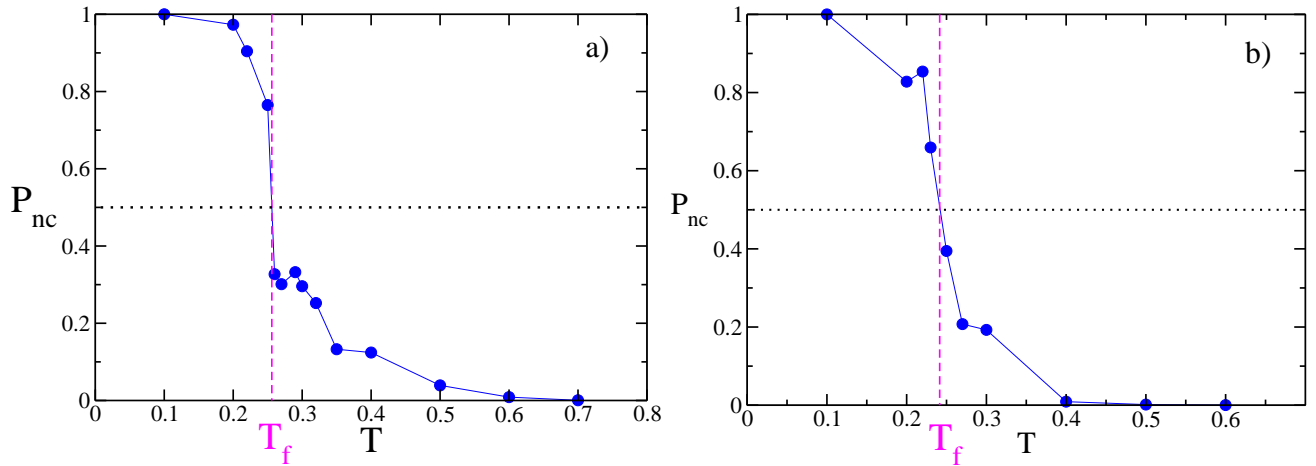


FIG. 2: (Color online) Probability P_{nc} as a function of the temperature T for good (a) and bad (b) folder; the vertical (magenta) dashed line indicates the folding temperature T_f , while the horizontal (black) dotted line refers to the value 0.5. .

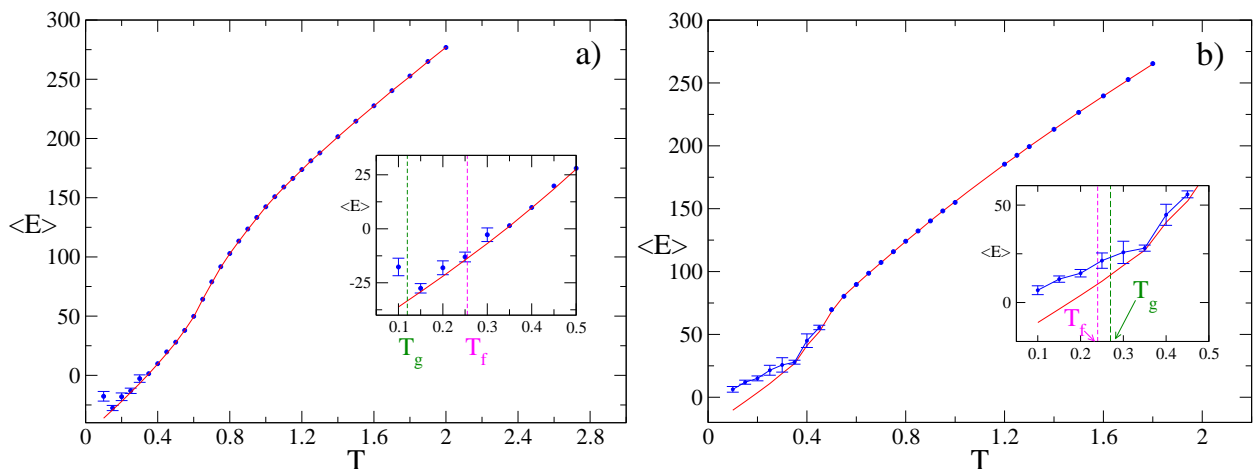


FIG. 3: (Color online) Total energy $\langle E \rangle$ as a function of the temperature T for good (a) and bad (b) folder; the solid (red) line corresponds to US's and the (blue) symbols to FS's. In the inset an enlargement for low temperatures: the dashed lines indicate the glassy (T_g) (magenta) and folding (T_f) (green) temperatures.

As shown, in Fig. 3, these quantities, when obtained from USs and FSs, coincide at temperatures larger than T_g , below which the structural arrest takes place. In particular, unfolding averages have been performed over intervals of duration $t = 10^5$ by following a single trajectory. On the other hand, folding simulations have been followed up to times $t \simeq 1.1 \cdot 10^7$ and the averages taken over 5-7 different initial conditions for considering for each trajectory only the last time span of duration $t \simeq 5 \cdot 10^4$. The error bars (standard deviation) shown in Fig. 3 should be interpreted, at sufficiently low temperatures, as a sign of the dependence of the results on the initial conditions.

	GF	BF
T_θ	0.65(1)	0.46(2)
T_f	0.255(5)	0.24(1)
T_g	0.12(2)	0.27(2)

TABLE III: Transition temperatures estimated for good and bad folder with the corresponding error.

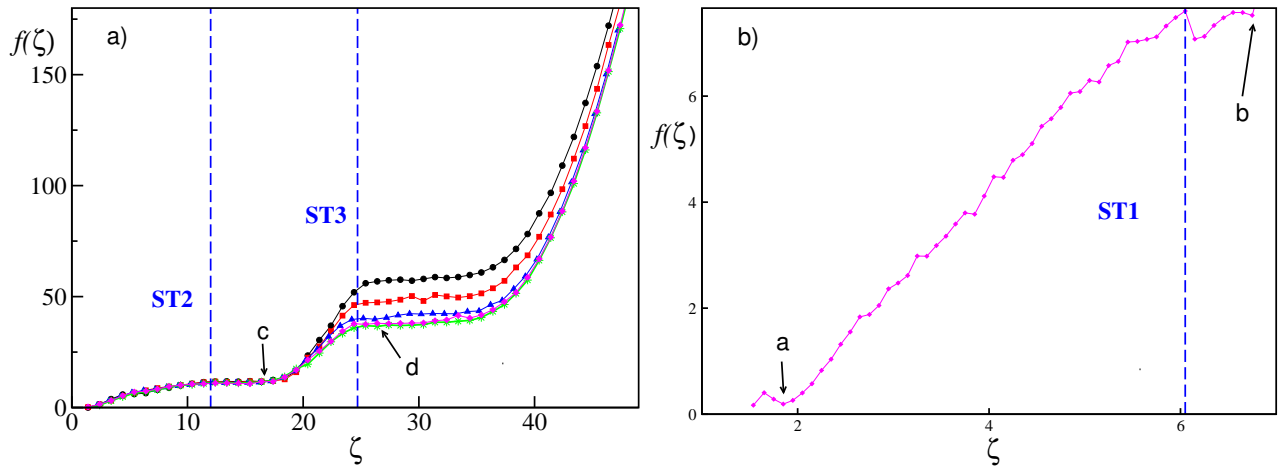


FIG. 4: (Color online) (a) Free energy profile f for the good folder as a function of the end-to-end distance ζ at $T = 0.3$, obtained with the EJE for various pulling velocities: from top to bottom $v_p = 5 \times 10^{-2}$, 1×10^{-2} , 5×10^{-3} , 5×10^{-4} and 2×10^{-4} . In (b) an enlargement of the curve for $v_p = 5 \times 10^{-4}$ at low ζ is reported. The number of different pulling experiments performed to estimate the profiles ranges between 150 and 250. The letters indicate the value of $f(\zeta)$ for the pulled configurations reported in Fig. 5 (a) and the (blue) dashed lines the location of the STs.

The three transition temperatures estimated for the good and bad folder are reported in table III ². One can notice that T_θ is larger for the good folder, thus indicating that the collapsed state has a greater stability with respect to the bad folder. Moreover, while for the good folder $T_f > T_g$, for the bad one this order is reversed. Therefore the BF will most likely remain trapped in some misfolded configurations before reaching the NC even at temperatures $T \sim T_f$.

VI. EXTENDED JARZYNSKI EQUALITY RECONSTRUCTION

In this section we present for both the sequences GF and BF the reconstruction of the FEL, at various temperatures, as a function of the end-to-end distance ζ . The free energy profiles have been obtained via the EJE by averaging over 100 – 250 repetitions of the same pulling protocol as described in section II B. We have generally used the pulling configuration where the first bead is kept fixed and the 46th bead is pulled (tail-pulled case). Moreover, in the Appendix we have also considered the head-pulled case, where the roles of the first and last bead are reversed.

A. Good folder

In Fig. 4 (a) is presented the EJE reconstruction for $T=0.3$ obtained at various pulling velocities for the good folder. As a first point, we notice that the estimated FEL (obtained for a number of repetitions between 150 and 250) collapses into an asymptotic curve as the pulling velocity decreases in agreement with the results reported in [43, 49]. In particular, for the good folder the asymptotic shape is already reached for $v_p = 5 \times 10^{-4}$. Moreover, referring to Fig. 4, it is possible to identify the structural transitions (STs) induced by the pulling experiment. As shown in Fig. 4 (b), the asymptotic $f(\zeta)$ profile exhibits a clear minimum in correspondence of the end-to-end distance of the NC (namely, $\zeta_0 \sim 1.9$). Moreover, up to $\zeta \sim 6$, the protein remains in native-like configurations characterized by a β -barrel made up of 4 strands, while the escape from the native valley is signaled by the small dip at $\zeta \sim 6$ and it is indicated as ST1 in Fig. 4 (b). This ST has been firstly identified in [37] by analyzing the the potential energy of ISs measured during a mechanical unfolding (numerical) experiment. In particular, Lacks [37] identifies this transition as an irreversible transition, in the sense that above this transition it is no more sufficient to reverse the stretching to

² In [29] for the sequence GF it has been found $T_\theta = 0.65$ and $T_f \sim 0.34$; moreover in the same paper the authors suggested that the folding transition was associated to a shoulder in the C , but this result has been recently criticized [36]. Moreover, more recent estimates, obtained by employing different protocols, suggest that $T_f \sim 0.24 - 0.25$ [8, 10] and $T_g \sim 0.15$ [10], values that are essentially in agreement with our results

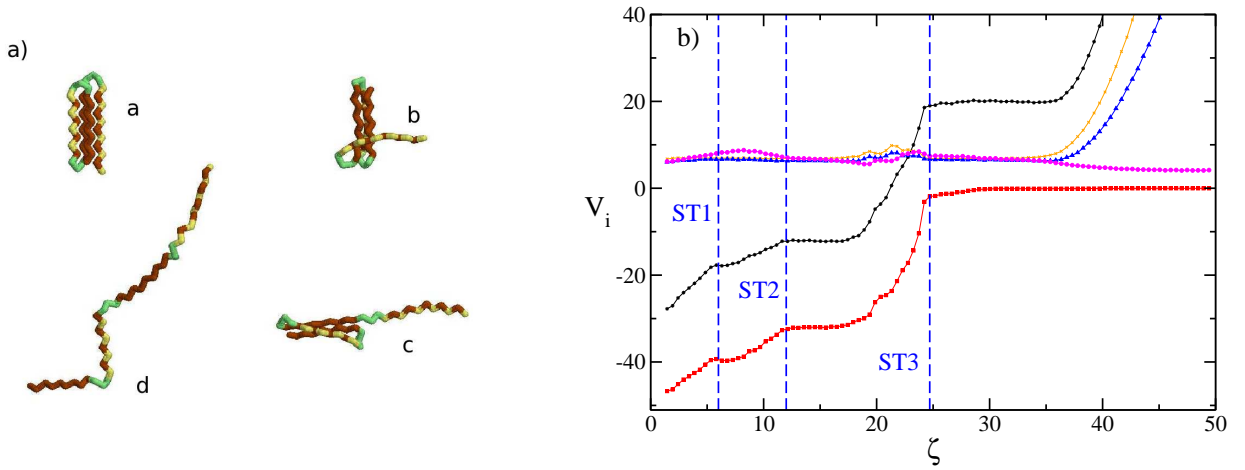


FIG. 5: (Color online) (a) Pulled configurations of the good folder at $T = 0.3$: the NC (a) has $\zeta_0 \sim 1.9$; the others are characterized by $\zeta = 6.8$ (b), $\zeta = 16.8$ (c), and $\zeta = 27.1$ (d). The beads of type N , B , and P are colored in green, red and yellow, respectively. (b) Potential energies contributions as a function of the end-to-end distance ζ estimated during a pulling experiment with speed $v_p = 5 \times 10^{-4}$ and obtained by averaging over 160 different realizations at $T = 0.3$. Black stars indicate the entire potential energy V , orange crosses V_1 , blue triangles V_2 , magenta diamonds V_3 , and red squares V_4 . The blue dashed lines indicate the transitions previously discussed in the text.

recover the previously visited configurations³.

For $\zeta > 6$ the configurations are characterized by an almost intact core (made of 3 strands) plus a stretched tail corresponding to the pulled fourth strand (see (b) in Fig. 5(a)). The second ST amounts to pull the strand $(PB)_5P$ out of the barrel. In the range $13 < \zeta < 18.5$ the curve $f(\zeta)$ appears as essentially flat, thus indicating that almost no work is needed to completely stretch the tail once detached from the barrel (see configuration (c) in Fig. 5(a)). The pulling of the third strand (that is part of the core of the NC) leads to a definitive destabilization of the β -barrel. This transition is denoted as ST3 in Fig. 4 (b). The second plateau in $f(\zeta)$ corresponds to protein structures made up of a single strand (similar to (d) in Fig. 5(a)).

To distinguish between entropic and energetic costs associated to each ST we have also evaluated separately the potential energy contributions V_i ($i = 1, \dots, 4$) during the pulling experiment, these data are reported in Fig. 5(b). From the figure it is clear that the variation of the potential energy during the stretching is essentially due to the Lennard-Jones term V_4 , while the other terms contribute in a much smaller amount, at least up to $\zeta \sim 35$. The transition ST1 has essentially only energetic costs, since $\Delta F = 8(1)$ and the potential energy varies almost of the same amount, in particular $\Delta V \sim \Delta V_4$. The other transitions instead have not negligible entropic costs, since the free energy barrier heights associate to ST2 and ST3 are 11(1) and 37(2), respectively; while the corresponding potential energy barriers are higher, namely $\Delta V = 16(1)$ for ST1 and $\Delta V = 49(1)$ for ST2. From Fig. 5(b) it is clear that above $\zeta \sim 35$, while the Lennard-Jones and dihedral contributions vanish, the final (almost quadratic) rise of the free energy is due to the harmonic and angular contributions, since we are now stretching bond distances and angles beyond their equilibrium values.

In Fig. 6 the reconstruction of the FEL obtained at various temperatures is shown. For temperatures around T_f one still observes a FEL resembling the one found for $T = 0.3$, while by increasing the temperature the dip around $\zeta \sim 6 - 7$ (associated to ST1) disappears and the heights of the other two barriers reduce. By approaching T_θ the first plateau, characterizing the transition from the NC to configurations of type (c), essentially disappears, and it is substituted by a monotonous increase of $f(\zeta)$. This suggests that 4 stranded β -barrel configurations coexist with partially unfolded ones. Above T_θ only one barrier remains indicating that at these temperatures the protein unfolds completely in one step process.

The connection between dynamical properties of the system and the free energy profile is still an open problem. In particular, the relationship between the unfolding times and the free energy barriers has been previously discussed in Ref. [48] for proteins and more recently the same problem has been addressed for Ising-like lattice protein model in

³ Please notice that we observe this transition at $\zeta \sim 6$ and not at $\zeta = 4.782$ as Lacks has reported, since we are considering the free energy profile at $T = 0.3$, while Lacks' analysis concerns potential energies of the ISs and some difference between the end-to-end distance of thermal configurations and of the underlying ISs should be expected [9].

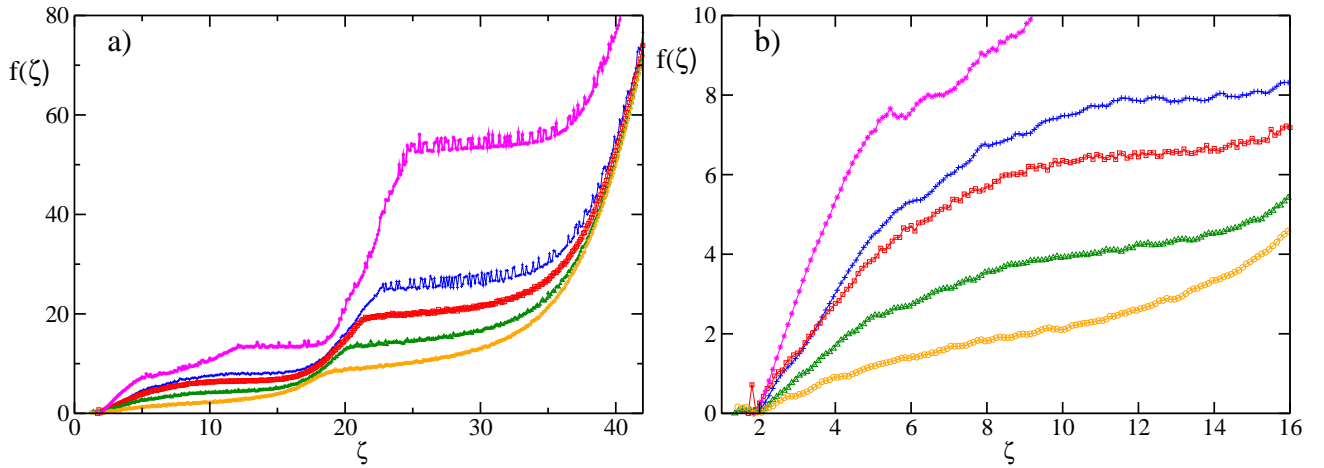


FIG. 6: (Color online) (a) Free energy profiles $f(\zeta)$ obtained with the EJE for good folder at various temperatures: $T = 0.2$ (magenta stars), 0.4 (blue plus), 0.5 (red squares), 0.6 (green triangles) and 0.7 (orange circles). In (b) an enlargement is reported at small ζ . Data refer to $v_p = 5 \times 10^{-4}$. The number of different realizations performed to estimate the averages at the different temperatures ranges between 160 and 250.

Ref. [49]. We have estimated average first passage times τ via USs by recording the time needed to the protein to reach a certain end-to-end threshold ζ_{th} once it starts from the NC at different temperatures. Our data, reported in Fig. 7, clearly indicate that at low temperatures the simple result of the transition state theory [50, 51, 52], namely

$$\tau = \frac{e^{\Delta f/T}}{T} \quad , \quad (31)$$

where $\Delta f = f(\zeta_{th}) - f(\zeta_0)$, is in very good agreement with the numerics. However, at high temperatures the agreement worsens. Therefore, in order to take in account all the details of the free energy profile and not only the barrier height, we have generalized a result of the Smoluchowski theory for the escape of a particle from a potential well [52] as follows [49]

$$\tau \propto \frac{1}{T} \int_{\zeta_0}^{\zeta_{th}} dy e^{f(y)/T} \int_{\zeta_0}^y dz e^{-f(z)/T} \quad (32)$$

where the potential energy has been substituted by the free energy profile. The estimation obtained via eq. (32) compare well with the numerical results at all the considered temperatures, unfortunately apart an arbitrary scaling factor common to all the temperatures that we are unable to estimate (see Fig. 7).

B. Bad Folder

In Fig. 8(a) are reported the free energy profiles reconstructed via the EJE at $T = 0.3$ for different pulling speeds, as in the case of the GF one observe a collapse to an asymptotic curve for a sufficiently small speed. At variance with the GF case, this speed is now ten times smaller, namely $v_p = 5 \times 10^{-5}$.

For the BF the mechanically induced unfolding transition are less clearly identifiable from the inspection of the free energy profile. Since for the BF not only the LJ interactions play a role in the STs but also the dihedral terms. Moreover, these two terms contribute with opposite signs to the whole potential energy thus partially canceling each other. Therefore, in order to identify the STs it is better to consider the distinct average profile of the single potential contributions V_i ($i = 1, \dots, 4$) reported in Fig. 8(b). In particular, the most relevant is the Lennard-Jones term V_4 , due to the stabilizing effect of the hydrophobic interactions on the protein structure. From the inspection of V_4 , at least four different STs can be single out, occurring at $\zeta \sim 7.3, 14.5, 23.6$, and 28.1 , respectively.

The first transition amounts to pull the last part of the tail out of the NC, namely the 6th and 5th strand that we have previously identified. To this ST is associated a free energy increase of $3.5(5)$ and a potential energy variation of $8.0(5)$, once the ST1 is completed the protein assumes the configuration (b) shown in Fig. 9. ST2 consists in pulling out from the compact configuration the whole tail (therefore to detach also the 4th strand) and leaving the protein in a configuration composed by the core (represented by the first three strands) plus a long tail (see configuration (c) in

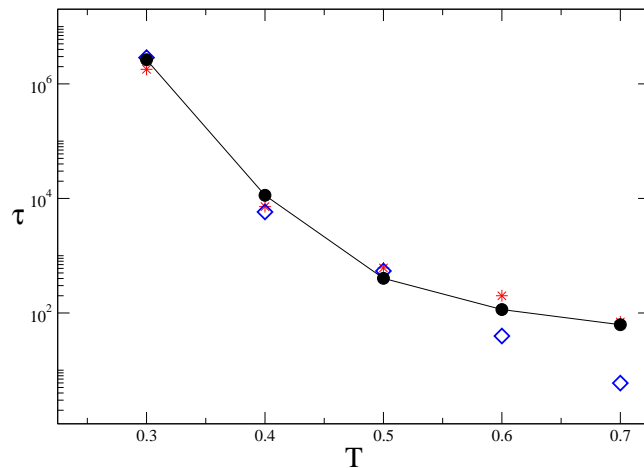


FIG. 7: (Color online) Average unfolding times τ for the GF at various temperatures corresponding to $\zeta_{th} = 4$. Filled (black) circles denote the numerical data, the estimations obtained via eq. (31) and eq. (32) are represented by empty (blue) diamonds and (red) stars, respectively. The arbitrary scaling factor entering in eq. (32) (see text) has been set equal to 8. The average times have been estimated over 100,000 – 200,000 unfolding events for $T = 0.7$ and 0.6, 12,000 events at $T = 0.5$ and as few as 200 and 60 events at the lowest temperatures, namely $T = 0.4$ and 0.3.

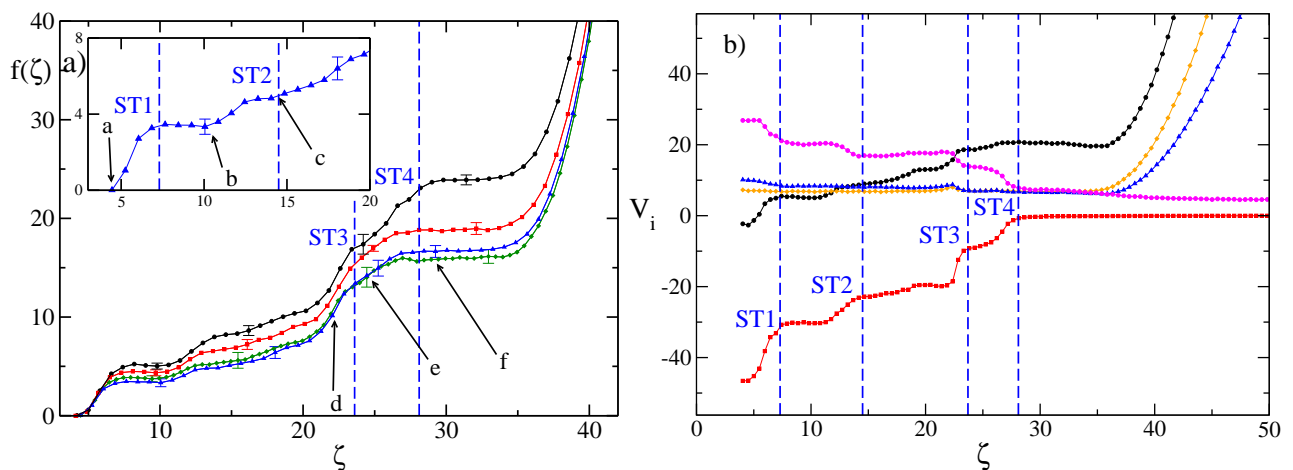


FIG. 8: (Color online) (a) Free energy profile f for the bad folder as a function of the end-to-end distance ζ , obtained with the EJE for various pulling velocities: from top to bottom $v_p = 5 \times 10^{-4}$ and 160 realizations (black circles), 2×10^{-4} and 200 realizations (red squares), 1×10^{-4} and 200 realizations (blue triangles), 5×10^{-5} and 100 realizations (green diamonds). In the inset an enlargement of the curve at low ζ for $v_p = 5 \times 10^{-5}$ is reported. The error bars indicate the amplitude of fluctuations among nearby channels. Data have been obtained at $T = 0.3$. (b) Potential energy contributions as a function of the end-to-end distance ζ estimated during a pulling experiment with velocity $v_p = 5 \times 10^{-5}$ and obtained by averaging over 100 different realizations at $T = 0.3$. Black stars indicate the entire potential energy V , orange crosses V_1 , blue triangles V_2 , magenta diamonds V_3 , and red squares V_4 . The magenta dashed lines indicate the transitions discussed in the text.

Fig. 9). The entropic contributions to ST2 is quite relevant since to pass from the NC to (c) the free energy increases of 5.5(5), while the associated potential energy variation is more than the double, i.e. 12(1). The third transition amounts to detach the first β -strand ($BNBPB_3NP$) from the core and this operation has much greater costs with respect to the previous STs, namely, $\Delta f = 13.5(1)$ and $\Delta V = 21(1)$. The complete opening of the core structure (now made only of the second and third strand) occurs at $\zeta \sim 28$ amounting to a total free (resp. potential) energy barrier to overcome of height 16(1) (resp. 23(1)). The total entropic costs for the GF and BF are of the same order, amounting roughly to one third of the energetic ones. However, for the BF their contribution is never negligible for all the four examined transitions. Finally, analogously to the GF for $\zeta > 35$ the LJ and dihedral contribution essentially vanishes and the free energy increase is due to the harmonic and angular terms, only.

In Fig. 10 the reconstruction of the FEL for the bad folder is reported at three temperatures below T_θ . As one can notice the bad folder exhibits at comparable temperatures much lower free energy barriers, indicating that the NC

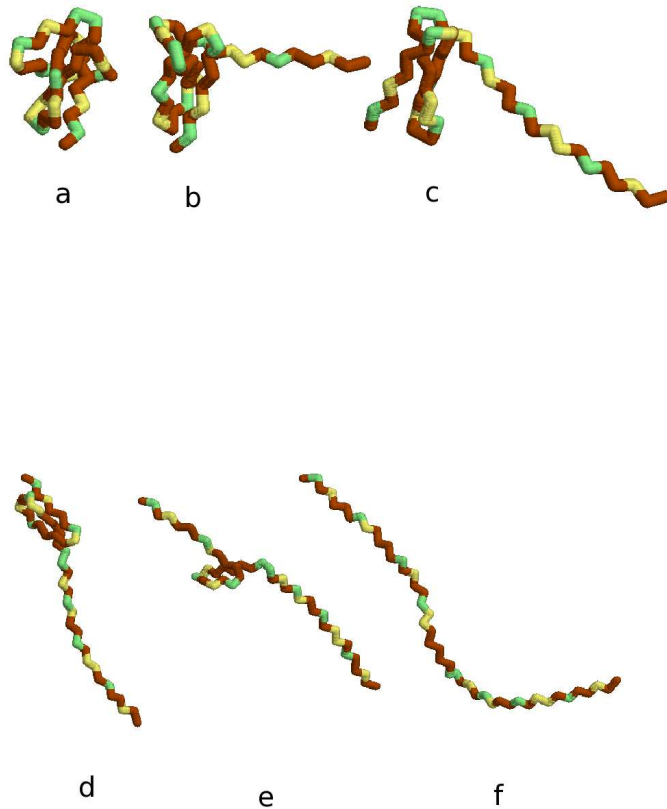


FIG. 9: (Color online) (a) Pulled configurations of the bad folder at $T = 0.3$: The configurations indicated in Fig. (a) refer to $\zeta_0 = 4.7$ (NC) (a), $\zeta = 9.9$ (b), 14.5 (c), 22.1 (d), 24.6 (e), and 29.7 (f)

and the partially folded structures are less stable, with respect to the GF. This is reflected also in the value of T_θ that has a smaller value with respect to the GF: namely, 0.46 for BF and 0.65 for GF. By increasing T the heights of the free energy barriers rapidly decrease and the various STs become less clearly defined.

VII. INHERENT STRUCTURE LANDSCAPE

In this section we compare the reconstructions of the FEL for the good and bad folder obtained with the EJE and with the IS approach. As already explained in Sect. III, we have created two IS data banks : the thermal data bank (TDB) obtained by performing equilibrium canonical simulations and the pulling data bank (PDB) by mechanically unfolding the protein.

In Fig. 11 is shown for the GF the comparison between $f_{IS}(\zeta)$ and the $f(\zeta)$ obtained via the EJE reconstruction at three temperatures. The results reveal an almost complete coincidence up to $\zeta \sim 5$, while for larger ζ , $f_{IS}(\zeta)$ slightly underestimates the free energy. By increasing T the disagreement somehow reduces, this is probably due to the fact that the thermal fluctuations favor a better exploration of the phase space and a better identification of the relevant ISs. The further comparison reported in Fig. 11 between the IS reconstructions obtained via the TDB and the PDB indicates a perfect coincidence up to $\zeta \sim 17$. On the contrary, during the last stage of the unfolding process the two f_{IS} differ: the TDB FEL is steeper than the PDB one. This suggests that during the mechanical unfolding the protein can easier reach states with low energies, even at large ζ . These states have a very low probability to be visited during thermal equilibrium dynamics. However, at $T = 0.3$ the value of the barrier to overcome and that of the final plateau are quite similar to those of the PDB FEL. Moreover, at higher temperatures the final energy plateaus of the TDB FEL are essentially coincident with the EJE free energy reconstruction. It should be remarked that the IS conformation with the maximal end-to-end distance is the all *trans*-configuration: an elongated (planar) equilibrium

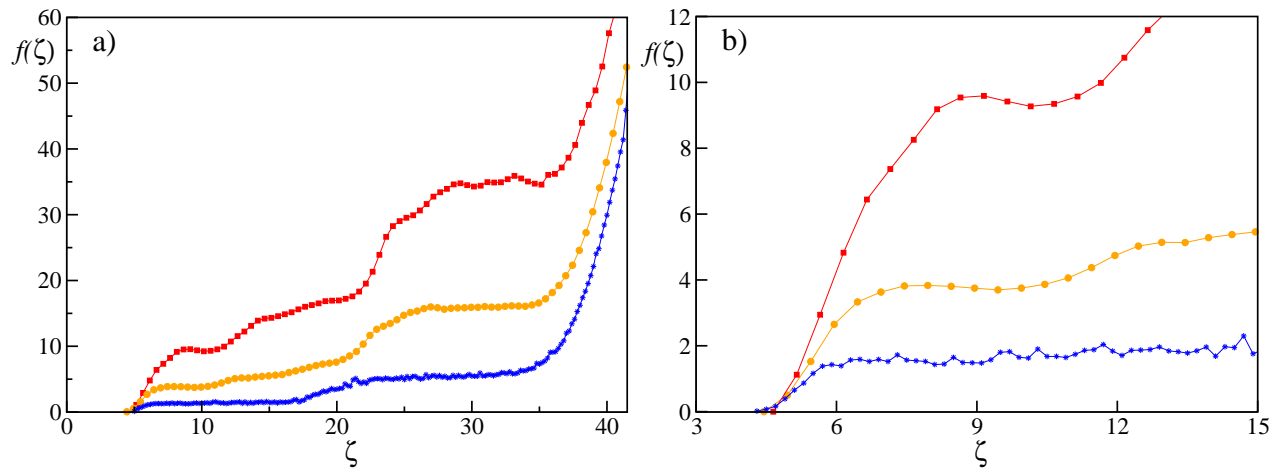


FIG. 10: (Color online) Free energy profiles obtained via the EJE for bad folder at three temperatures: namely, $T = 0.2$ for $v_p \sim 2 \times 10^{-4}$ (red squares), $T = 0.3$ for $v_p \sim 5 \times 10^{-5}$ (orange circles), $T = 0.4$ for $v_p \sim 2 \times 10^{-4}$ (blue stars). In (b) an enlargement is reported at small ζ . Data refer to averages performed over 100-250 samples of the same protocol.

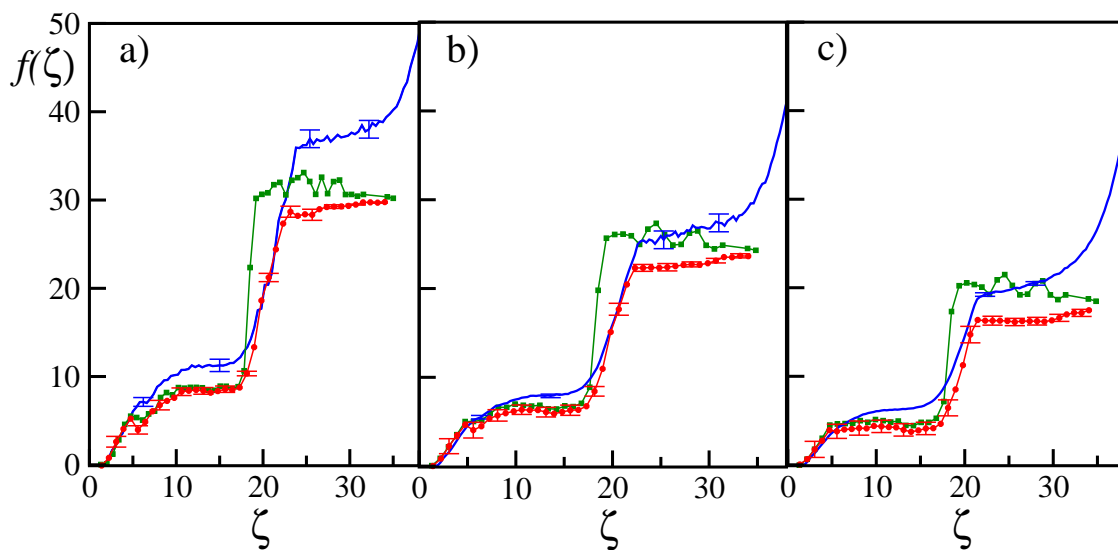


FIG. 11: (Color online) Free energy profiles as a function of ζ for various temperatures and number of repetitions of the pulling experiments for the good folder: a) $T = 0.3$ and 160 repetitions; b) $T = 0.4$ and 240 experiments; c) $T = 0.5$ and 240 repetitions. The blue solid line refers to the EJE reconstruction $f(\zeta)$ for $v_p = 5 \times 10^{-4}$, green squares to $f_{IS}(\zeta)$ obtained by employing the TDB and red circles to $f_{IS}(\zeta)$ obtained by employing the ISs in the PDB for each considered T .

conformation of the protein with all the dihedral angles at their *trans* values. This corresponds to $\zeta_{trans} = 35.70$, therefore the IS approach does not allow to evaluate the FEL for $\zeta > \zeta_{trans}$. For the GF, we can safely affirm that the out-of-equilibrium process consisting in stretching the protein is more efficient to investigate the FEL, since a much smaller number of ISs are needed to reliably reconstruct it (at least up to $\zeta \sim 17$), as reported in Table II.

The comparison for the BF case is reported in Fig. 12 at $T = 0.1, 0.2$ and 0.3 . Also in this case the $f_{IS}(\zeta)$ and the $f(\zeta)$ coincide up to $\zeta \sim 5$, however above such value the IS reconstruction is really poor, apart at the higher temperature, namely $T = 0.3$, where it is acceptable up to $\zeta \sim 20$. In this case the agreement between the two IS reconstructions is quite good at any considered temperature and ζ . The differences with respect to the GF case can be ascribed to the fact that the protein can now easily visit attraction basins of ISs characterized by a quite broad range of end-to-end distance. To better understand this point we have performed USs for the GF and BF for $T_g \lesssim T \lesssim T_\theta$ and we have estimated the average, the minimal and the maximal ζ associated to the visited ISs. The corresponding data are reported in Fig. 13. While for the GF the minimal value remains essentially ζ_0 for all the temperatures and the maximum ζ increases smoothly up to ~ 18 at $T = T_\theta$, the dependence of the minimal and maximal ζ -values on T are more dramatic for the BF. Up to the temperatures $T \sim 0.5 \times T_\theta$, average, minimal and maximal ζ -values almost

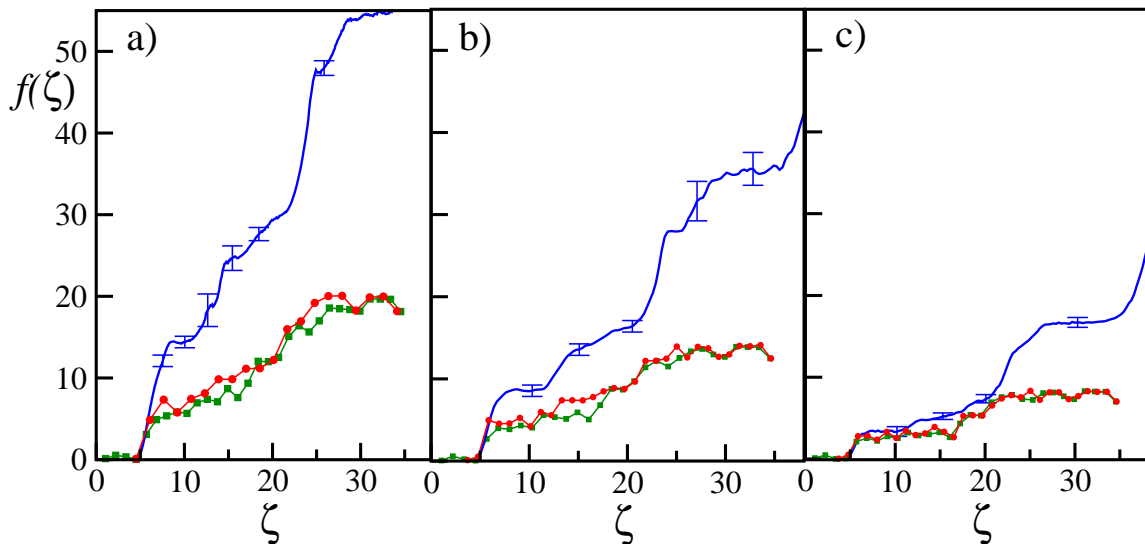


FIG. 12: (Color online) Free energy profiles as a function of ζ for various temperatures for the bad folder: a) $T = 0.1$ with $v_p = 1 \times 10^{-4}$ and 120 pulling experiments; b) $T = 0.2$ with $v_p = 2 \times 10^{-4}$ and 240 experiments; c) $T = 0.3$ with $v_p = 5 \times 10^{-5}$ and 100 experiments. The symbols are the same as in Fig. 11, the EJE reconstructions appear as asymptotic at the employed pulling velocities.

coincide indicating that the protein is still confined around the NC, please remember that for the BF $T_g = 0.58 \times T_\theta$. As soon as $T > 0.6 \times T_\theta$ the maximum grows abruptly and reach the upper bound corresponding to ζ_{trans} already at $T \sim T_\theta$, on the other hand the minimum value decreases indicating that at higher temperatures the protein can access basins of ISs with end-to-end distance lower than ζ_0 . This last result indicates that there is not a clear monotonic correspondence between the temperature increase and the achievable protein extensions. Moreover, the fact that the protein can easily attain also extremely stretched configurations at not too high temperatures suggests that in the case of the BF the protein can easily escape from the native valley and reach any part of the phase space, while for the GF the accessible IS configurations were much more limited at comparable temperatures. Therefore, the fact that the IS reconstruction fails to reproduce the actual equilibrium FEL already at not too large ζ can be considered as a further indication of the bad foldability properties of the BF sequence.

The origin of the residual differences between the IS and EJE reconstruction observable for the GF, are not completely clear. The observed discrepancies seem not to be (mainly) due neither to the convergence problems of the EJE approach to the equilibrium free energy nor to the harmonic approximation employed to estimate the vibrational term (10) entering in the IS reconstruction. The quality of the convergence is assessed by the fact that the collapse of the curves towards an asymptotic profile (see Fig. 4(a)) is already reached at the pulling velocities v_p employed in our analysis. Furthermore, the observed differences are larger than the error bars due to the lack of convergence, displayed with the EJE reconstruction in Fig. 11. Moreover, the harmonic approximation employed to estimate the vibrational term (10) seems to be quite good for the GF up to $T = 0.6$, as already pointed out in [10] by considering the average potential energy. Here, we perform a more detailed comparison to verify the validity of the harmonic approximation. In particular, we directly evaluate the IS partition function by estimating the probabilities $P_a(T)$ to visit the metastable minima of the potential energy during an equilibrium canonical simulation at temperature T . We sample the trajectory at constant time intervals $\delta t = 1$ and we identify the corresponding ISs by employing a quasi-Newton scheme. As suggested in [9], in order to improve the sampling of the energy landscape, particularly at low temperatures, we can perform a unique US at a quite high temperature T_{ref} and derived the partition function at any T as follows:

$$\bar{Z}_{IS}(\zeta, T) \equiv e^{-\beta \bar{f}_{IS}(\zeta, T)} = \sum_a' \frac{P(V_a, T_{ref}) e^{-V_a/T}}{e^{-V_a/T_{ref}}} \quad (33)$$

where the sum is restricted to the ISs with end-to-end distance within the narrow interval $[\zeta, \zeta + d\zeta]$.

An optimal choice for T_{ref} is the θ -temperature, because by operating at this temperature the molecular dynamics trajectory is able to sample both folded and unfolded structures. The comparison between f_{IS} obtained by employing the TDB plus the harmonic approximation and \bar{f}_{IS} is reported in Fig. 14 for the GF and BF at various temperatures. For the GF the agreement between the two estimations is quite good up to $T = 0.5$ in the interval $\zeta_0 < \zeta < 18.5$.

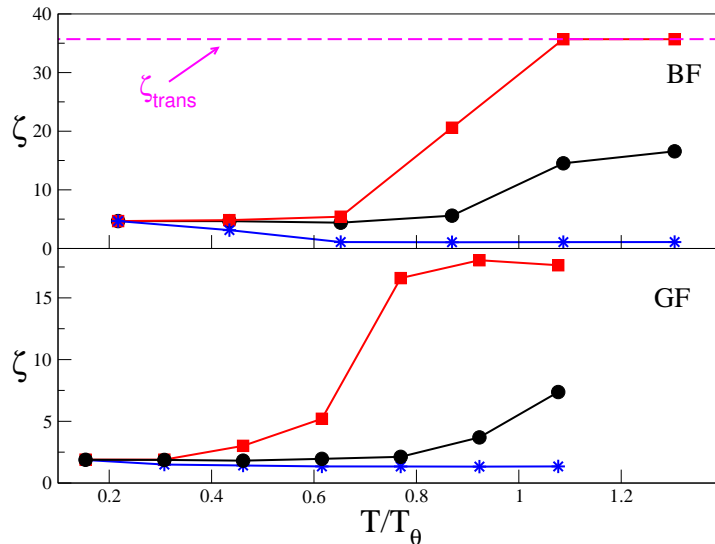


FIG. 13: (Color online) End-to-end distance of the ISs estimated during USs at various temperatures: (black) circles represent the average value; (blue) stars the minimal value; and (red) squares the maximal one. The upper panel refer to the BF and the lower one to the GF. The horizontal magenta dashed line indicates the ζ_{trans} -value. For the GF (resp. BF) trajectories of duration $t \sim 100,000 - 500,000$ (resp. $t \sim 50,000 - 250,000$) have been examined to obtain the ISs at constant time intervals $\Delta t = 5$.

Unfortunately, at the considered $T_{ref} = 0.65$ the maximal reachable elongation takes the value $\zeta \sim 18.5$ and no information can be obtained for larger end-to-end distances. For the BF we report only the comparison for $T = 0.3$, however the agreement between f_{IS} and \bar{f}_{IS} is good for all the examined ζ and for temperatures as large as $T = 0.4$. At $T = 0.5$ for the GF some discrepancies is indeed present. Moreover, this analysis confirms once more that for the BF there is a complete accessibility of the whole phase space up to ζ_{trans} already at $T \sim T_\theta$, while this is not the case for the GF. We can therefore conclude that the disagreement between the EJE and IS reconstructions of the FEL is probably due to the fact that the IS analysis is based only on minima of the potential, while the saddles are completely neglected from this picture.

Moreover, from the IS analysis by employing Eq. (14) we can obtain an estimate of the profiles of the potential and vibrational free energies $V_{IS}(\zeta)$ and $R_{IS}(\zeta)$, respectively. From the latter quantity, the entropic costs associated to the various unfolding stages can be estimated. As shown in Fig. 15(a), for the GF at $T = 0.3$, the structural transitions ST2 and ST3 previously described correspond to clear "entropic" barriers, while the ST1 transition has only energetic costs since $\Delta R_{IS} \sim 0$. This last result is in perfect agreement with the previously reported EJE analysis. For what concerns the other two transitions, ST2 is associated to a decrease $\sim 6(1)$ of $R_{IS}(\zeta)$ once more in agreement with the EJE reconstruction. For ST3 the analysis discussed in Sect. VIA indicates a vibrational free energy barrier $\sim 12(2)$, while $\Delta R_{IS}(\zeta) \sim 15(2)$ is slightly larger. Moreover, the reconstructed potential energies $V_{IS}(\zeta)$ are in very good agreement with the average potential energy evaluated during the corresponding pulling experiments as shown in Fig. 15, apart around ST1. At this transition $V_{IS}(\zeta)$ exhibits a barrier followed by a clear minimum, while the average potential energy V reveals a smooth and continuous increase. However, the potential energy barrier is essentially the same within the error bars.

Finally, one can try to put in correspondence the three unfolding stages previously discussed for the GF with thermodynamical aspects of the protein folding. In particular, by considering the energy profile $V_{IS}(\zeta)$, an energy barrier ΔV_{IS} and a typical transition temperature $T_t = (2\Delta V_{IS})/(3N)$ can be associated to each of the STs. The first transition ST1 corresponds to a barrier to overcome $\Delta V_{IS} = 8(1)$ and therefore to $T_t = 0.11(1)$, that, within error bars, coincide with T_g . For the ST2 transition the barrier to overcome is $\Delta V_{IS} = 16(1)$ and this is associated to a temperature $T_t \simeq 0.23(2)$ (slightly smaller than T_f). The energetic cost to completely stretch the protein is $50(1)$ with an associated transition temperature $T_t = 0.72(1)$, that is not too far from the θ -temperature. At least for the GF, our results indicate that the observed STs induced by pulling can be put in direct relationship with the thermal transitions usually identified for the folding/unfolding process.

For the BF the IS approach is able to well reproduce the average potential energy during the pulling experiment as clearly shown in Fig. 15(b), however the estimation of the "entropic" barriers gives a quite large overestimation of those associated to the structural transitions. In particular, at $T = 0.3$ the vibrational free energy barrier to overcome to complete unfold the BF obtained by the EJE reconstruction is $8(2)$, while the corresponding decrease of R_{IS} is

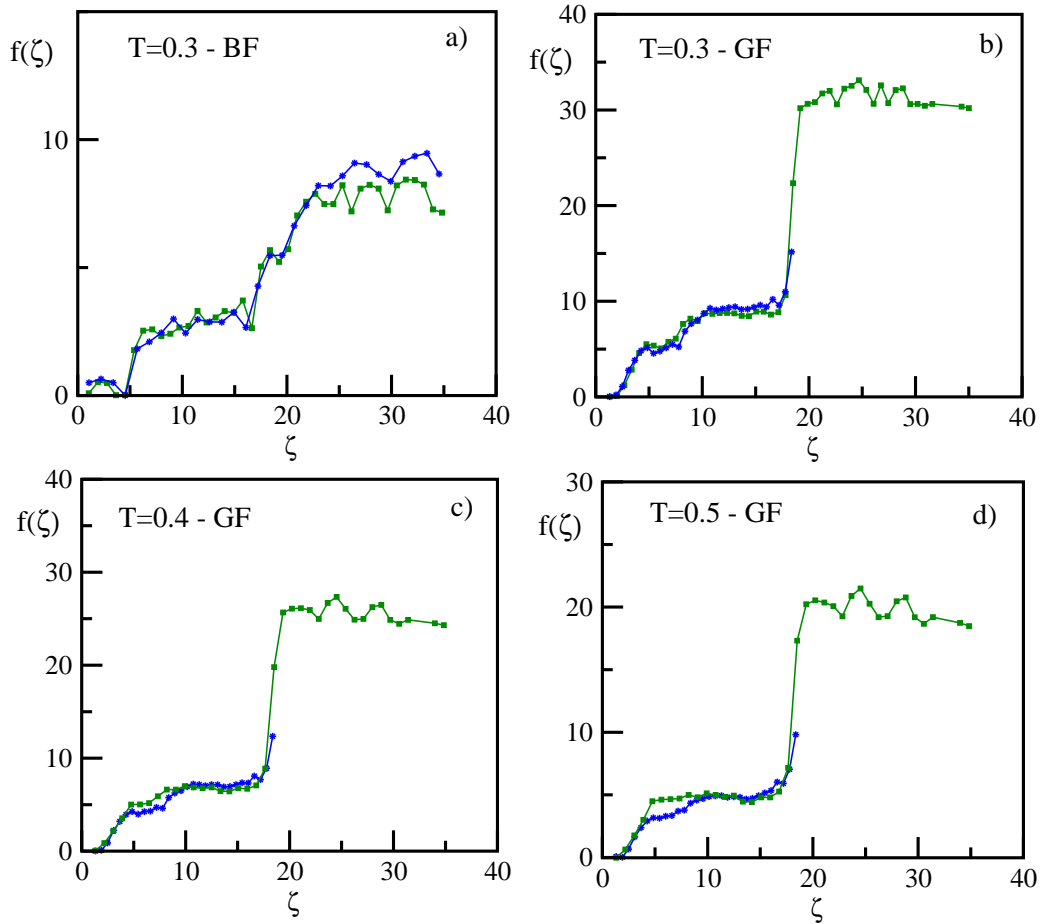


FIG. 14: (Color online) Comparison of f_{IS} obtained by employing the TDB (green circles) and \bar{f}_{IS} (blue stars) at various temperatures for the GF (with $T_{ref} = 0.65$) and the BF (with $T_{ref} = 0.5$). For the estimation of \bar{f}_{IS} , $\sim 320,000$ (resp. $\sim 450,000$) minima have been collected for the GF (resp. BF).

the double, i.e 16(1). This overestimation of the vibrational free energy term R_{IS} , in particular for ζ larger than ~ 17 , is at the origin of the observed discrepancies between the IS and EJE reconstructions for the BF. However, as shown in Fig. 14 (a) this cannot be due to the employed harmonic approximation, neither to relaxation problems of the EJE analysis. Therefore, this seems to point out that for the BF the unfolding paths passing in proximity of saddles (not considered in the IS approach) are more relevant than for the GF. The free energy depends more heavily on entropic contributions different from the vibrational ones: large structural rearrangements being already possible at temperatures as low as $T = 0.3$ as testified from Fig. 13. Since in this case the unfolding dynamics cannot be well described by the knowledge of the ISs and of the oscillations (at the bottom) of the corresponding attraction basins, we cannot expect to infer any information on the thermal transitions from the knowledge of the potential energy barriers at the STs, as done for the GF. Indeed the estimated transition temperatures T_t for the four examined structural transitions give values not corresponding to any of the relevant temperatures reported in Table III for the BF.

VIII. CONCLUDING REMARKS

In conclusion, the quality of the comparison of the EJE and IS reconstructions of the free energy landscape performed for the good and bad folder sequences are quite different. For the good folder we can safely affirm that the information obtained by the equilibrium FEL both with the EJE and the IS methodologies are consistent and give substantiated hints about the thermal unfolding. On the other hand for the bad folder the IS approach seems somehow to fail and the discrepancy seems related to the fact that entropic contributions associated to large conformational rearrangement are not reproducible within the IS framework. In other terms the unfolding process for the good folder consists of

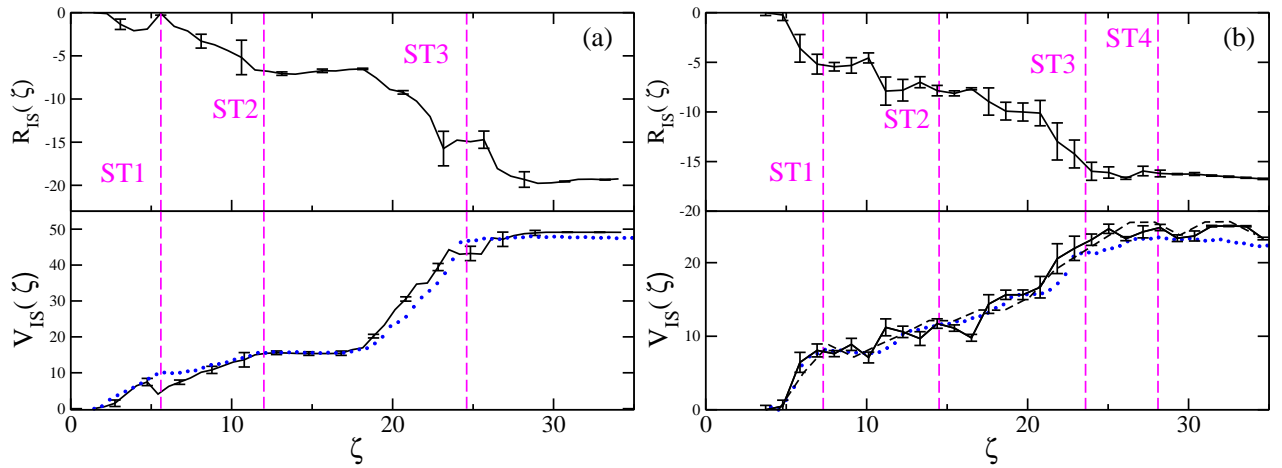


FIG. 15: (Color online) Reconstructed $V_{IS}(\zeta)$ (lower panel) and $R_{IS}(\zeta)$ (upper panel) for good folder (a) and bad folder (b) by employing ISs in the PDB at $T = 0.3$. In the lower panel the blue dotted line refers to the average potential energy evaluated during the corresponding pulling experiments (this has been already reported in Fig. 5(b) for the GF and in Fig. 8(b)) for the BF. In the lower panel in (b) the black dashed line refers to $T = 0.1$. Please notice that the data have been vertically translated in order to have zero energy at the NC.

many small successive rearrangements of the NC, which are well captured by the corresponding ISs. While for the bad folder the unfolding takes place via large conformational modifications, not sufficiently well reproduced by the IS picture. The unfolding transition is characterized by a dynamics evolving in a landscape dominated by minima for the good folder, while for the bad folder it occurs in a scenario where unstable saddles play a fundamental role.

For the good folder, the quality of the free energy landscape reconstruction via the extended Jarzinsky equality can be well appreciated by stressing that from pure structural information about the landscape a good estimate of dynamical quantities, like the unfolding times from the native configuration, can be obtained. Moreover, the agreement of the results obtained with the two approaches indicates that these two methodologies can be fruitfully integrated to provide complementary information on the protein landscape. In particular the investigation of the ISs allows us to give an estimate of the (free) energetic and entropic barriers separating the native state from the completely stretched configuration. These barriers are associated to the structural transition induced by the protein manipulation, but for the good folder they can put in direct relationship with the thermal transitions usually identified during folding/unfolding processes.

Future work on more realistic heteropolymer models is needed to clarify if the observed features, distinguishing good folders from bad folders, can be really considered as a specific trademark of proteins.

Acknowledgments

Useful discussions are acknowledged with L. Bongini, L. Casetti, L. Delfini, S. Lepri, R. Lima, R. Livi, L. Peliti, A. Politi, A. Rampioni, F. Sbrana, L. Tsimiring, and M. Vassalli. In particular, the field potential here employed has been developed by A. Rampioni during his PhD thesis in collaboration with L. Bongini, R. Livi, A. Politi and one of the authors (AT). We acknowledge CINECA in Bologna and INFN for providing us access to the Beowulf Linux cluster under the Grant Iniziativa Calcolo Parallelo. This work has been partially supported by the European Community via the STREP project EMBIO NEST Contract No. 12835.

APPENDIX A: TAIL-PULLING VERSUS HEAD-PULLING

Since recent experimental results have shown that the pulling geometry influences the mechanical resistance of a protein [17], besides the usual pulling configuration (tail-pulled case) we have also considered a situation where the role of the first and last bead are reversed (head-pulled case). In Fig. 16, the results obtained for the tail and head-pulled configuration are compared: we find that the free energy profiles for GF and BF, obtained at $T = 0.3$ by employing the largest speeds ensuring asymptotic results, are identical. This implies that for the considered pulling speed the mechanical unfolding pathways are the same, namely the various strands of the protein open up following the same

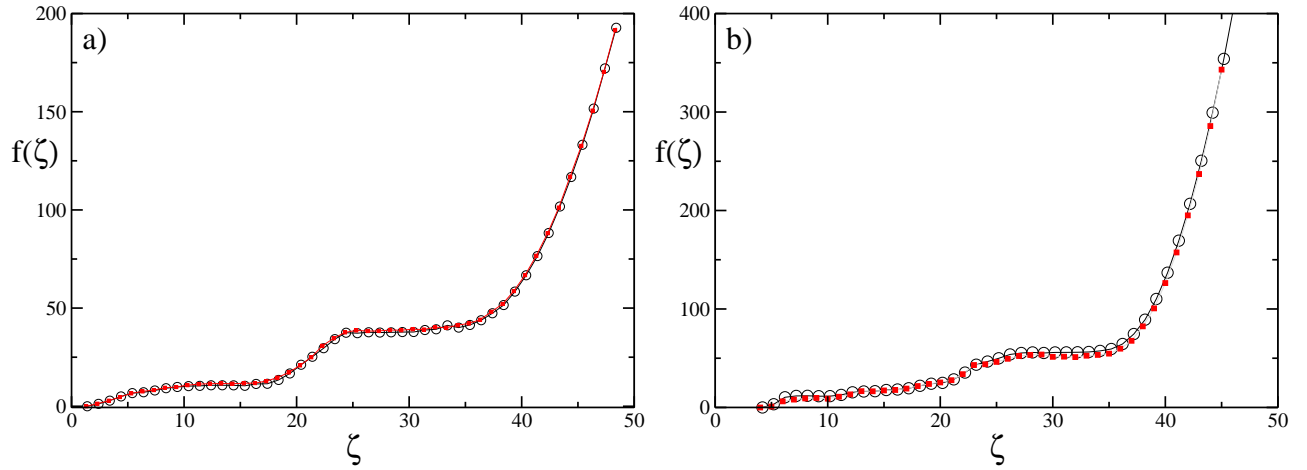


FIG. 16: (Color online) Comparison of the EJE reconstruction of the free energy profile for good folder in the tail-pulled (open black circles) and head-pulled (red squares) case. (a) Good folder sequence at $T=0.3$ and $v_p = 5 \times 10^{-4}$; (b) bad folder sequence at $T = 0.3$ and $v_p = 5 \times 10^{-5}$.

rupture order in both cases. These findings essentially agree with those reported in [38] where the authors have found that the sequence of unfolding events depends on pulling velocities and temperature, moreover they observe that the strands open in the same order for sufficiently low pulling velocities and temperatures⁴. This result can be considered as a further confirmation that the asymptotic FEL obtained via the EJE reconstruction is indeed the equilibrium one.

-
- [1] D.J. Wales, *Energy Landscapes*, Cambridge University Press, Cambridge, 2003.
[2] F.H. Stillinger and T.A. Weber, *Science* **225** (1984) 983.
[3] S. Sastry, P.G. Debenedetti, and F.H. Stillinger, *Nature* **393** (1998) 554.
[4] L. Angelani, R. Di Leonardo, G. Ruocco, A. Scala, and F. Sciortino, *Phys. Rev. Lett.* **85** (2000) 5356.
[5] T.S. Grigera, A. Cavagna, I. Giardina, and G. Parisi, *Phys. Rev. Lett.* **88** (2002) 055502.
[6] M.A. Miller and D.J. Wales, *J. Chem. Phys.* **111** (1999) 6610; P.N. Mortenson and D.J. Wales, *J. Chem. Phys.* **114** (2001) 6443; P.N. Mortenson, D.A. Evans and D.J. Wales, *J. Chem. Phys.* **117** (2002) 1363.
[7] S.V. Krivov and M. Karplus, *J. Chem. Phys.* **117** (2002) 10894.
[8] D.A. Evans and D.J. Wales, *J. Chem. Phys.* **118** (2003) 3891.
[9] N. Nakagawa and M. Peyrard, *Proc. Natl. Acad. Sci. USA* **103** (2006) 5279; *Phys. Rev. E* **74** (2006) 041916.
[10] J. Kim and T. Keyes, *J. Phys. Chem. B* **111** (2007) 2647
[11] A. Baumketner, J.-E. Shea, and Y. Hiwatari, *Phys. Rev. E* **67** (2003) 011912.
[12] D.A. Evans and D.J. Wales, *J. Chem. Phys.* **121** (2004) 1080.
[13] P.E. Leopold, M. Montal, and J.N. Onuchic, *Proc. Natl. Acad. Sci. USA* **89** (1992) 8721.
[14] M. Carrion-Vazquez *et al.* *Proc. Natl. Acad. Sci. USA* **96** (1999) 3694; B. Onoa *et al.*, *Science* **299** (2003) 1892.
[15] M. Carrion-Vazquez *et al.*, *Nat. Struct. Biol.* **10** (2003) 738.
[16] A. Irbäck, S. Mitternacht, and S. Mohanty, *Proc. Natl. Acad. Sci. USA* **102** (2005) 13427.
[17] D.J. Brockwell *et al.*, *Nature Structural Biology* **10** (2003) 731.
[18] A. Imparato and L. Peliti, *Eur. Phys. J. B* **39** (2004) 357.
[19] C. Jarzynski *Phys. Rev. Lett.*, **78** (1997) 2690; G.E. Crooks *Phys. Rev. E* **60** (1999) 2721.
[20] D. Collin *et al.*, *Nature* **437** (2005) 231.
[21] D.K. West, P.O. Olmsted, and E. Paci, *J. Chem. Phys.* **125** (2006) 204910.
[22] G. Hummer and A. Szabo, *Proc. Natl. Acad. Sci. USA* **98**, 3658 (2001).
[23] T. Speck and U. Seifert, *Phys. Rev. E*, **70**, 066112 (2004).
[24] A. Imparato and L. Peliti, *Europhys. Lett.*, **70**, 740-746 (2005).
[25] A. Imparato and L. Peliti, *Phys. Rev. E*, **72**, 046114 (2005).
-

⁴ The lowest pulling velocity analyzed by the authors in Ref. [38] for the GF was $v_p = 0.36\text{m/s}$ while the lowest temperature was $T = 20\text{K}$. In our adimensional units these values correspond to $v_p \simeq 2.3 \times 10^{-3}$ and $T \simeq 0.17$. Therefore we are considering a much smaller speed, but a somehow larger temperature. For a comparison with physical units see [35].

- [26] N.C. Harris, Y. Song, and C.-H. Kiang, *Phys. Rev. Lett.* **99** 068101 (2007)
- [27] A. Imparato, S. Luccioli, and A. Torcini, *Phys. Rev. Lett.* **99** (2007) 168101.
- [28] Z. Guo and D. Thirumalai, *Biopolymers*, **36** (1995) 83.
- [29] Z. Guo and C.L. Brooks III, *Biopolymers*, **42** (1997) 745-757.
- [30] S. Fowler *et al.*, *J. Mol. Biol.* **322** (2002) 841.
- [31] E. Paci and M. Karplus, *Proc. Natl. Acad. Sci. USA* **97** (2000) 6521.
- [32] D.K. West, P.O. Olmsted, and E. Paci, *J. Chem. Phys.* **124** (2004) 144909.
- [33] J.D. Honeycutt and D. Thirumalai, *Proc. Natl. Acad. Sci. U.S.A.* **87** (1990) 3526.
- [34] R.S. Berry, N. Elmaci, J.P. Rose, and B. Vekhter, *Proc. Natl. Acad. Sci. U.S.A.* **94** (1997) 9520.
- [35] T. Veitshans, D. Klimov, and D. Thirumalai, *Folding & Design* **2** (1997) 1.
- [36] J. Kim, J.E. Straub, and T. Keyes, *Phys. Rev. Lett.* **97** (2006) 050601.
- [37] D.J. Lacks, *Biophys. J.* **88** (2005) 3494.
- [38] F.-Y. Li, J.-M. Yuan, and C.-Y. Mou, *Phys. Rev. E* **63** (2001) 021905
- [39] A. Blondel and M. Karplus, *J. Computational Chemistry*, **17** (1996) 1132-1141.
- [40] A. Rampioni, *Caratterizzazione del panorama energetico di piccoli peptidi al variare della loro lunghezza*, PhD Thesis (Firenze, 2005)
- [41] W. Kabsch, *Acta Cryst.* **A32** (1976). 922-923
- [42] W.H. Press *et al.*, *Numerical Recipes* (Cambridge University Press, 1994, New York).
- [43] A. Imparato and L. Peliti, *J. Stat. Mech.* (2006) P03005.
- [44] Braun, A. Hanke, and U. Seifert, *Phys. Rev. Lett* **93** (2004) 158105.
- [45] A. Torcini, R. Livi, and A. Politi, *J. Biol. Phys.* **27** (2001) 181.
- [46] L. Bongini, R. Livi, A. Politi, and A. Torcini, *Phys. Rev. E* **68** (2003) 061111; *ibidem* **72** (2005) 051929.
- [47] P-G De Gennes, *Scaling Concepts in Polymer Physics* (Cornell University Press, 1979).
- [48] D.K. West, P.O. Olmsted, and E. Paci, *Phys. Rev. E* **74** (2006) 061912.
- [49] A. Imparato, A. Pelizzola, and M. Zamparo, *Phys. Rev. Lett.* **98** 148102 (2007)
- [50] J.S. Langer, *Ann. Phys.* **54** (1969) 258
- [51] P. Hänggi, P. Talkner, and M. Borkovec, *Rev. Mod. Phys.* **62** (1990) 251.
- [52] R. Zwanzig, *Nonequilibrium statistical mechanics* (Oxford University Press, 2001)